Cationic state distribution over the chlorophyll *d*-containing P_{D1}/P_{D2} pair in photosystem II

Keisuke Saito [1], Jian-Ren Shen [2], and Hiroshi Ishikita [1,3]*

1) 202 Building E, Career-Path Promotion Unit for Young Life Scientists, Graduate School of Medicine, Kyoto University, Yoshida-Konoe-cho, Sakyo-ku, Kyoto 606-8501, Japan

2) Division of Bioscience, Graduate School of Natural Science and Technology/Faculty of Science, Okayama University, Okayama 700-8530, Japan.

3) Japan Science and Technology Agency (JST), PRESTO, 4-1-8 Honcho Kawaguchi, Saitama 332-0012, Japan

CORRESPONDING AUTHOR: Hiroshi Ishikita, 202 Building E, Career-Path Promotion Unit for Young Life Scientists, Graduate School of Medicine, Kyoto University, Yoshida-Konoe-cho, Sakyo-ku, Kyoto 606-8501, Japan, Tel. +81-75-753-9286, Fax. +81-75-753-9286, **E-mail:** hiro@cp.kyoto-u.ac.jp

Abbreviations:

A. marina, Acaryochloris marina; Chl, chlorophyll; OEC, oxygen-evolving cluster; PSII, photosystem II; QM/MM approach, quantum mechanical/molecular mechanical approach; *T. elongatus*, *Thermosynechococcus elongatus*; *T. vulcanus, Thermosynechococcus vulcanus*

Abstract

Most of the chlorophyll (Chl) cofactors in photosystem II (PSII) from *Acaryochloris marina* are Chl*d*, although a few Chl*a* molecules are also present. To evaluate the possibility that Chl*a* may participate in the P_{D1}/P_{D2} Chl pair in PSII from *A. marina*, the $P_{D1}^{\bullet+}/P_{D2}^{\bullet+}$ charge ratio was investigated using the PSII crystal structure analyzed at 1.9-Å resolution, while considering all possibilities for the Chl*d*-containing P_{D1}/P_{D2} pair, i.e., Chl*d*/Chl*d*, Chl*a*/Chl*d*, and Chl*d*/Chl*a* pairs. Chl*d*/Chl*d* and Chl*a*/Chl*d* pairs resulted in a large $P_{D1}^{\bullet+}$ population relative to $P_{D2}^{\bullet+}$, as identified in Chl*a*/Chl*a* homodimer pairs in PSII from other species, e.g., *Thermosynechococcus elongatus* PSII. However, the Chl*d*/Chl*a* pair possessed a $P_{D1}^{\bullet+}/P_{D2}^{\bullet+}$ ratio of approximately 50/50, which is in contrast to previous spectroscopic studies on *A. marina* PSII. The present results strongly exclude the possibility that the Chl*d*/Chl*a* pair serves as P_{D1}/P_{D2} in *A. marina* PSII.

Keywords: Photosystem II, chlorophyll *d*, spin density distribution, *Acaryochloris marina*, redox potential, P680

1. INTRODUCTION

The reaction center of photosystem II (PSII) is composed of a D1/D2 heterodimer, harboring the chlorophyll *a* (Chl*a*) pair P_{D1}/P_{D2}, the accessory Chl*a* Chl_{D1}/Chl_{D2}, two pheophytin *a* $Pheo_{D1}/Pheo_{D2}$, two quinones, and two additional Chl*a* $Chl_{Z(D1)}/Chl_{Z(D2)}$ molecules as redox active cofactors. P680, which absorbs light at a wavelength of 680 nm, is formed among these Chl*a* molecules. Excitation of P680 leads to the formation of the $Chl_{D1}^{\bullet+}$ $Pheo_{D1}^{\bullet-}$ state [1-3], followed by the $[P_{D1}/P_{D2}]^{\bullet+}$ $Pheo_{D1}^{\bullet-}$ state. The resulting $[P_{D1}/P_{D2}]^{\bullet+}$ state serves as an electron abstractor for the oxygen-evolving complex (OEC). Thus, water oxidation is ultimately achieved by the high redox potential for one-electron oxidation (E_m) of P680. To date, the E_m(P680) value has not been directly measured in experimental studies. Instead, the E_m(P680) value has been estimated mainly from measured E_m values of other cofactors. The E_m(P680) value was first estimated to be 1.1 V by Klimov et al. in 1979 on the basis of the E_m value of pheophytin, measured as -0.61 V at pH 11 [4]. Subsequently, Rutherford et al. supported this claim, also estimating that the E_m(P680) value was 1.1 V [5]. In contrast, very low E_m(P680) values, between 0.8 and 0.9 V, were reported by Watanabe, Kobayashi, and colleagues [6-8]. After the PSII crystal structure from *Thermosynechococcus elongatus* was reported with 3.8-Å resolution [9], Rappaport et al. estimated that the E_m(P680) was 1.26 V [10], based on measurement of the $E_m(Q_A)$ (approximated to be -30 mV by Rutherford, Krieger, and colleagues [11, 12]) in PSII from *Synechocystis* PCC 6803 [10]. This measurement was higher than previously reported [4, 5]. In 2005, Grabolle and Dau reported a similar value of 1.25 V [13]. On the basis of the PSII crystal structure at 3.0-Å resolution [14], Ishikita et al. reported $E_m(P_{D1})$ and $E_m(P_{D2})$, .i.e., E_m for the Chl*a* monomer, to be 1.1–1.2 V by solving the linearized Poisson-Boltzmann equation and considering the protonation states of all titratable sites [15]. Recently, Kato et al. reported that the E_m(P680) was 1.17–1.21 V, extrapolated from an $E_m(Pheo_{D1})$ value of -0.5 V [16] measured at physiological pH (6.5) in PSII from *T. elongatus*. From these studies, it appears that the E_m(P680) value reaches 1.1–1.2 V (reviewed in Refs. [17-20]), a value significantly higher than the E_m of monomeric Chl*a* in organic solvents.

Following initial charge separation in the reaction center of PSII, the positive charge is distributed over P_{D1}/P_{D2}, resulting in a $P_{D1}^{\bullet+}/P_{D2}^{\bullet+}$ state. The $P_{D1}^{\bullet+}/P_{D2}^{\bullet+}$ ratio (or the corresponding spin density distribution) was reported to be 82/18 from ENDOR studies of spinach PSII [21] or 80/20 from flash-induced spectroscopic studies of *Synechocystis* PCC 6803 PSII [22], suggesting a preferential localization of the cationic state on P_{D1} over P_{D2}, irrespective of the high similarity in D1 and D2 protein sequences [23]. The cause of the asymmetric distribution of the cationic state has been attributed mainly to the electrostatic asymmetry of the D1/D2 residue pairs due to the presence of the OEC and associated functions in the D1 protein subunit side (secondary to the geometrical asymmetry of P_{D1}/P_{D2} chlorophylls) [24]; this is in contrast to the cationic state distribution of the corresponding Chl pair in PSI [25].

Chl*d* is the major Chl pigment in *Acaryochloris marina* (making up more than 95% of the Chl pigments), although some Chl*a* (less than 5%) is also present [26-29]. In *A. marina* grown under high iron conditions, the pigment content per 2 pheophytin *a* (i.e., $Pheo_{D1}$ and $Pheo_{D2}$) was estimated to be 1.4 Chl*a* [29]. Recent studies have suggested that the pigment stoichiometry of 2 pheophytin *a* in the *A. marina* PSII comprises 29.6 ± 1.2 Chl*d* and 1.9 ± 0.1 Chl*a* molecules [30]. Although the majority of the Chl is Chl*d*, characteristic for the *A. marina* PSII, the origin of the minor Chl (Chl*a*) is a serious question. Chl*d* and Chl*a* differ geometrically in their chemical group at the $C3^1$ atom position; Chl*d* possesses a formyl group at this position, whereas Chl*a* possesses a vinyl group (Figure 1).

There is no direct evidence demonstrating that Chl*a* is actually located in the reaction center of the *A. marina* PSII (see statements in Ref. [31]). However, observation of the accumulation of the cationic state on a single Chl*a* molecule (i.e., bleaching at 435 nm and increase in absorption at 820 nm) in *A. marina* PSII by Schlodder et al. [31] should be considered, particularly in terms of the fact that prior studies have shown the accumulation of a cationic state specifically at P_{D1} in PSII from spinach [21], *Synechocystis* PCC 6803 [22], and *T. elongatus* [32, 33] (note that although no clear statement was

made describing a large population specifically consisting of $P_{D1}^{\bullet+}$ in Refs. [32, 33], it was reasonable to assume the presence of this population from Ref. [24]). Thus, Schlodder et al. proposed that P_{D1}/P_{D2} is a Chl*a*/Chl*d* heterodimer [31, 34]. In addition, Cser et al. [35] concluded that the measured $E_m(Pheo_{D1})$ value in the *A. marina* PSII was the same as that in Chl*a* type PSII and proposed that Chl*a* was involved in the primary donor of the *A. marina* PSII. To unambiguously confirm this, however, one must clarify how the P_{D1}/P_{D2} moiety of the *A. marina* PSII is able to discriminate between the minor species Chl*a* and the major species Chl*d* and specifically uptake a Chl*a* molecule at the P_{D1} position.

On the other hand, Tomo et al. proposed that P_{D1}/P_{D2} is a Chl*d*/Chl*d* homodimer [36, 37]. An advantage of the Chl*d*/Chl*d* homodimer model is that Chl*d* is the major species in the *A. marina* PSII, and thus, this model does not have to rationalize the specificity of Chl*a* at P_{D1}. In contrast to the results by Cser et al. [35], Tomo et al. [36] or Allakhverdiev et al. [38] observed that $E_m(Pheo_{D1})$ in the *A. marina* PSII was by ~80 mV higher than in the *Synechocystis* PCC 6803 PSII. Interestingly, the experimentally measured E_m value for Chl*d* in DMF is ~70 mV higher than that of Chl*a* [39]. The essentially same shift as observed in the $E_m(Pheo_{D1})$ difference between the two PSII proteins suggests the energetic conservation of light-induced charge separation and water oxidation among PSII species including the Chl*d*-containing P_{D1}/P_{D2} pair, preferring the Chl*d*/Chl*d* homodimer model over the Chl*a*/Chl*d* heterodimer model [38]. To support the Chl*d*/Chl*d* homodimer model, the researchers also presented light-induced Fourier transform infrared (FTIR) spectra of both the *A. marina* PSII and the *Synechocystis* PCC 6803 PSII [36]. The 1100–1800 cm^{-1} region of the *A. marina* PSII clearly indicates that approximately 80% of the cationic state was localized on a single Chl. Based on the high similarity of the D1/D2 protein sequences between the *A. marina* PSII and, for instance, the *T. elongatus* PSII (Figure S1, supporting information), the cationic state is likely to be more populated on P_{D1} than P_{D2}. Thus, one can conclude that the $P_{D1}^{\bullet+}/P_{D2}^{\bullet+}$ ratio is approximately 80/20 for the *A. marina* PSII, as observed in PSII from spinach [21], *Synechocystis* PCC 6803 [22], and *T. elongatus* [32, 33]. Because the CH stretching vibration of a formyl group corresponds to a peak at approximately 2700 cm^{-1} (See

Refs. [36, 40, 41] and Refs. therein), it would be helpful to investigate this region to distinguish between Chl*a* and Chl*d* in P_{D1}/P_{D2}. However, the absorbance in this region is approximately 10 times weaker than that of the 1100–1800 cm^{-1} region of the *A. marina* PSII [36] (and also in the *A. marina* PSI [40, 41]), making it difficult to assess and adding to the debate on P_{D1}/P_{D2} Chl models in the *A. marina* PSII.

All of these debates ultimately arise from the lack of structural information for the *A. marina* PSII. The exact molecular geometry surrounding the P_{D1}/P_{D2} Chl in the *A. marina* PSII remains unknown due to the lack of a crystal structure. Since the *A. marina* PSII possesses a high degree of D1 and D2 protein sequence similarity to the *T. vulcanus* PSII or the *T. elongatus* PSII (Figure S1, supporting information), we investigated the relationship between a possible Chl pair at the P_{D1}/P_{D2} position (i.e., Chl*d*/Chl*d*, Chl*a*/Chl*d*, and Chl*d*/Chl*a*) and the cationic state charge distribution over the P_{D1}/P_{D2} pair, using the *T. vulcanus* PSII crystal structure analyzed at a 1.9-Å resolution [42]. To calculate the $P_{D1}^{\bullet+}/P_{D2}^{\bullet+}$ ratio for the P_{D1}/P_{D2} Chl dimer, we used a large-scale quantum mechanical/molecular mechanical (QM/MM) approach, with the explicit treatment of the complete PSII atomic coordinates, defining the P_{D1}/P_{D2} dimer as the QM region and the remaining protein subunits-cofactors as the MM region. Thus, the entire P_{D1}/P_{D2} molecule is considered quantumchemically in the presence of the PSII electrostatic protein environment.

To avoid an uncertain prediction of the protein structure, we used the original protein atomic coordinates of the *T. vulcanus* PSII crystal structure [42], without performing homology modeling for the *A. marina* PSII. The present results should be interpreted within this limiting condition. Nevertheless, the present procedure is currently the best option for investigating this phenomenon in the absence of high-resolution crystal structures of the *A. marina* PSII. Although the identity of the amino acid sequence of the D1 protein, e.g., the region at 191 to 210 near the axial ligand of P_{D1} (i.e., D1-His198) is 80%, not specifically high, there is essentially no significant difference in their electrostatic characters (e.g., no [charged residue]/[uncharged residue] difference at the corresponding position in the two D1 proteins), which will not affect the $P_{D1}^{\bullet+}/P_{D2}^{\bullet+}$ energetics. Indeed, it has been suggested that the

structure of the PSII reaction center is similar to the PSII in Chl*a* organisms (See Ref. [31] and Refs. therein). In the *A. marina* PSII, delayed fluorescence from Chl*a* was observed as a result of charge recombination [36, 43], which may suggest that Chl_{D1} should be also investigated together with P_{D1}/P_{D2} (i.e., in terms of Chl_{D1} as an initial donor in PSII [1-3]). Due to the large system size, we did not include Chl_{D1} and Chl_{D2} in the QM region. Nevertheless, to the best of our knowledge, this is the first study that clearly demonstrates the cationic charge distribution and spin density distribution over all possible combinations of Chl*d* and/or Chl*a* pairs at the P_{D1}/P_{D2} position in the PSII protein environment.

2. METHODS

As demonstrated in the previous article [24, 25], we employed the following systematic modeling procedure: We constructed a realistic molecular model of the whole PSII complex using the resent high-resolution crystal structure. To obtain deeper insight into the electronic structure of P_{D1}/P_{D2} Chl dimer, which is the key molecule of the photosystem II reaction center, we performed large-scale QM/MM calculations for the entire PSII complex. Technical details of each modeling procedure are identical to those used in previous studies on PSII [24] and PSI [25] and summarized as follows.

2.1. Coordinates. The atomic coordinates of PSII were taken from the X-ray structure of the PSII complexes from *T. vulcanus* at 1.9 Å resolution (PDB ID: 3ARC) [42]. Hydrogen atoms were generated and energetically optimized with CHARMM [44], whereas the positions of all non-hydrogen atoms were fixed, and all titratable groups were kept in their standard protonation states, i.e., acidic groups were ionized and basic groups were protonated. For the QM/MM calculations, we added additional counter ions to neutralize the whole system. To avoid unnecessary artifacts of the protein side chain geometry, we used the original protein atomic coordinates of the *T. vulcanus* PSII crystal structure [42], without performing homology modeling of the *A. marina* PSII. Accordingly, atomic coordinates of the cofactors expect for the P_{D1}/P_{D2} Chl pair were kept as in the original *T. vulcanus* PSII crystal structure.

2.2. Atomic partial charges. Atomic partial charges of the amino acids were adopted from the all-atom CHARMM22 [45] parameter set. The charges of the protonated acidic O atoms were increased symmetrically by +0.5 unit charges to implicitly account for the presence of a proton. Similarly, instead of removing a proton in the deprotonated state, the charges of all of the protons of the basic groups of Arg and Lys were diminished symmetrically by a total unit charge. For residues for which the protonation states were not available in the CHARMM22 parameter set, appropriate charges were computed [46]. For the cofactors (e.g., the OEC cluster, Chl*a*, Pheo*a*, and quinones), the same atomic charges as in previous computations of PSII [24] were used.

2.3. OEC models. In the S_1-state, the valences of the 4 Mn atoms are most probably (III, III, IV, IV). The exact valences of the individual Mn atoms are unclear; however, we found that changing the charge distribution of each Mn atom from the above distribution did not affect our calculation results significantly [24]. The protonation states of the O atoms (and thus the net charge of the OEC atoms) in the OEC cluster remain unclear. Although O1, O2, and O3 are likely to be unprotonated O^{2-} based on observations of the OEC geometry, the protonation states of O4 linking Mn4 and Mn3 in the Mn_3CaO_4-cubane, and O5 in one of the corners of the cubane linking Mn4 and the cubane, necessitate more deep investigation as they might be O^{2-}, protonated OH^-, or even H_2O. Due to the uncertainty, we evaluated all possible combinations of the O4 and O5 protonation states and we tentatively used the $O4H^-$ $O5H^-$ model (see Ref. [24] for further details).

Except for a few examples [47], the spin coupling of the Mn ions has not been considered in a number of studies where the PSII protein environment was explicitly modeled (e.g., recent QM/MM studies on the S1-state model of OEC by Batista, Brudvig, and coworkers [48]). In particular, (i) our focus is not on the OEC cluster, (ii) the OEC cluster was included in the MM region (see below [24]), and (iii) the atomic charges of OEC do not differ significantly among the different spin structures [47]. Thus, the spin coupling was not considered in the present study.

2.4. QM/MM calculations. In all QM/MM calculations reported here, we employed the so-called electrostatic embedding QM/MM scheme. In all QM/MM calculations, we used the Qsite [49] program code. Electrostatic as well as steric effects created by complex PSII architecture were explicitly considered in all present calculations. Due to the large system size of PSII, the QM region was limited to the P_{D1}/P_{D2} Chl dimer for simplicity, while other protein units and all co-factors were approximated by the MM force field. Since we have optimized the atomic partial charges for the OEC cluster, Chl*a*, Pheo*a*, and quinones, the present QM/MM partition was accurate enough to describe the electronic structure of the $[P_{D1}/P_{D2}]^{\bullet+}$ Chl dimer. To reliably determine the cationic character of $[P_{D1}/P_{D2}]^{\bullet+}$ Chl dimer, we employed the unrestricted DFT method with the B3LYP functional and LACVP* basis sets. The detailed geometry of $[P_{D1}/P_{D2}]^{\bullet+}$ Chl dimer was refined by the constrained QM/MM optimizations; the surrounding protein environment was considered as the MM whose atomistic coordinates were exactly fixed with the original X-ray coordinates. After obtaining the stable geometry of QM fragment, we then determined the ESP charges for the cationic state of $[P_{D1}/P_{D2}]^{\bullet+}$ Chl dimer in the presence of the entire PSII atomic coordinates. (Table S1, Supporting Information).

3. RESULTS AND DISCUSSION

3.1. Orientation of the formyl group in Chl*d*. Chl*d* molecules at the P_{D1}/P_{D2} position were modeled by replacing the vinyl group of Chl*a* in the *T. vulcanus* PSII crystal structure with a formyl group. The position of this newly-introduced formyl group of Chl*d* was refined by the constrained QM/MM optimizations in the PSII protein environment as described above. Two orientations of the formyl group were energetically stable; one with the carbonyl O atom being oriented to the C5 H atom (Figure 2a) and another one with the formyl group flipped along the C3-$C3^1$ axis (Figure 2b).

The former orientation was slightly (by ~3 kcal/mol) more stable than the latter the monomeric form of Chl*d* in vacuum. In contrast, in the PSII protein environment, the latter orientation was always slightly (by ~3 kcal/mol) more stable than the former in all cases investigated, i.e., the dimeric form

(Chl*a*/Chl*d*, Chl*d*/Chl*a*, and Chl*d*/Chl*d*). Hence, the conformer in Figure 2a is advantageous in terms of intramolecular interaction energy (i.e., monomeric Chl itself) because the negative charge of the formyl O atom can be more stabilized by the proximity of the positive charge of the C5 H atom. On the other hand, in the P_{D1}/P_{D2} pair, the conformer in Figure 2b appears to be slightly advantageous in terms of the intermolecular energy (i.e., interaction with another Chl. We will not focus on elucidation of further details in the present study.). Thus, we focused on the latter orientation of the Chl*d* formyl group (Figure 2a) to investigate the cationic state distribution over the P_{D1}/P_{D2} pair in the PSII protein environment.

The formyl groups of P_{D1} and P_{D2} were located at a van der Waals distance (~3.5 Å) from D1-Met183/D2-Leu182 and D1-Phe206/D2-Leu206 in the geometry of the *T. vulcanus* PSII (Table S1, supporting information). These residue pairs correspond to Met/Leu and Leu/Leu in the D1/D2 protein sequences of the *A. marina* PSII, respectively (Figure S1, supporting information). Although it has been reported that the presence of an H bond partner for Chl affects the distribution of the cationic (spin) state over the Chl pair (e.g., in PSI [25, 50]), the present analysis suggests that the formyl groups will not possess H-bond partners in the *A. marina* PSII.

3.2. $P_{D1}^{\bullet+}/P_{D2}^{\bullet+}$ ratio. Tomo et al. proposed that the P_{D1}/P_{D2} pair in the *A. Marina* PSII was composed of a Chl*d*/Chl*d* pair [36]. The corresponding calculated $P_{D1}^{\bullet+}/P_{D2}^{\bullet+}$ ratio for the Chl*d*/Chl*d* pair was 76.5/23.5 in the whole PSII (Table 1), which is essentially the same as that of the Chl*a*/Chl*a* pair previously reported for the *T. vulcanus* PSII (76.9/23.1 [24]). The Chl*a*/Chl*d* pair, which was proposed by Schlodder et al. as the P_{D1}/P_{D2} pair in the *A. Marina* PSII [31], also resulted in a similar $P_{D1}^{\bullet+}/P_{D2}^{\bullet+}$ ratio of 85.1/14.9 (Table 1).

On the other hand, the Chl*d*/Chl*a* pair resulted in a $P_{D1}^{\bullet+}/P_{D2}^{\bullet+}$ ratio of approximately 50/50 (Table 1). Such a ratio was not proposed by Tomo et al. [36] or Schlodder et al. [31]. Because the cationic state distribution over the Chl pair is associated with the redox potentials for the E_m of the 2 Chl monomers [24, 25, 51, 52], similar amounts for the $P_{D1}^{\bullet+}$ and $P_{D2}^{\bullet+}$ populations imply that the E_m values of the 2

monomeric P_{D1} (Chl*d*) and P_{D2} (Ch*la*) Chls are also similar. The experimentally measured E_m value for Chl*d* in DMF is approximately 70 mV higher than that of Chl*a* [39]. This E_m difference between Chl*d* and Chl*a* is almost in the same range as the E_m difference between P_{D1} and P_{D2}, previously measured as 70–100 mV in the *T. vulcanus* PSII [24]. Thus, a Chl*d*/Chl*a* pair should yield isoenergetic E_m values for the 2 monomeric Chls. Thus, we can conclude that the Chl*d*/Chl*a* pair is unlikely to represent the P_{D1}/P_{D2} pair in the *A. marina* PSII.

Hence, it appears that both the Chl*d*/Chl*d* pair [36] and the Chl*a*/Chl*d* pair [31] are still possible candidates for the P_{D1}/P_{D2} pair in the *A. Marina* PSII. The reported localization of approximately 70%–80% of the cationic state on P_{D1} in FTIR studies by Tomo et al. [36, 37] is in accordance with the calculated $P_{D1}^{\bullet+}/P_{D2}^{\bullet+}$ ratio for the Chl*d*/Chl*d* pair in the present study (Table 1). However, the observed cationic state localization on a single Chl*a* that was attributed to P_{D1} in studies by Schlodder et al. [31] also agrees with our calculated $P_{D1}^{\bullet+}/P_{D2}^{\bullet+}$ ratio for the Chl*a*/Chl*d* pair (Table 1). These subtle differences in the $P_{D1}^{\bullet+}/P_{D2}^{\bullet+}$ ratios between the Chl*d*/Chl*d* pair and the Chl*a*/Chl*d* pair still make it difficult to determine the configuration of the relevant Chl pair in the *A. marina* PSII.

4. CONCLUSIONS

$P_{D1}^{\bullet+}/P_{D2}^{\bullet+}$ ratios for the Chl*d*/Chl*d* pair or the Chl*a*/Chl*d* pair in the *T. vulcanus* PSII environment were calculated to be 76.5/23.5 or 85.1/14.9, respectively, rendering a large $P_{D1}^{\bullet+}$ population relative to the $P_{D2}^{\bullet+}$ population. On the other hand, the Chl*d*/Chl*a* pair resulted in a symmetrically charged population over the two P_{D1} and P_{D2} monomers (56.7/43.3). The present results strongly suggest that the Chl*d*/Chl*a* pair is unlikely to serve as P_{D1}/P_{D2} in *A. marina* PSII. Further detailed studies, preferably on crystal structures of the *A. marina* PSII are required to unambiguously confirm the P_{D1}/P_{D2} pair to be either Chl*d*/Chl*d* or Chl*a*/Chl*d*.

5. ACKNOWLEDGMENT

This research was supported by the JST PRESTO program (H.I), Grant-in-Aid for Scientific Research from the Ministry of Education, Culture, Sports, Science and Technology (MEXT) of Japan (21770163

to H.I. and 22740276 to K.S.), Special Coordination Fund (H.I) for Promoting Science and Technology of MEXT, Takeda Science Foundation (H.I.), Kyoto University Step-up Grant-in-Aid for young scientists (H. I.), and Grant for Basic Science Research Projects from The Sumitomo Foundation (H. I.).

6. REFERENCES

[1] V.I. Prokhorenko and A.R. Holzwarth, Primary process and structure of the photosystem II reaction center: a photon echo study, J. Phys. Chem. B 104 (2000) 11563-11578.

[2] B.A. Diner and F. Rappaport, Structure dynamics, and energetics of the primary photochemistry of photosystem II of oxygenic photosynthesis, Annu. Rev. Plant Biol. 53 (2002) 551-580.

[3] G. Renger and T. Renger, Photosystem II: The machinery of photosynthetic water splitting, Photosynth Res 98 (2008) 53-80.

[4] V.V. Klimov, S.I. Allakhverdiev, S. Demeter and A.A. Krasnovskii, Photoreduction of pheophytin in the photosystem 2 of chloroplasts with respect to the redox potential of the medium, Dokl Akad Nauk SSSR 249 (1979) 227-230.

[5] A.W. Rutherford, J.E. Mullet and A.R. Crofts, Measurement of the midpoint potential of the pheophytin acceptor of photosystem II, FEBS Lett. 123 (1981) 235-237.

[6] T. Watanabe and M. Kobayashi, Electrochemistry of chlorophylls, in Chlorophylls (Scheer, H., Ed.) (1991) pp 287-303, CRC Press, Boca Raton, FL.

[7] S. Ohashi, T. Iemura, H. Miyashita, T. Watanabe and M. Kobayashi, New scheme for O_2 evolution in PSII, Photomed Photobiol 30 (2008) 13-18.

[8] M. Kobayashi, S. Ohashi, S. Fukuyo, M. Kasahara and T. Watanabe, The oxidation potential of Chl*a* is the lowest : a new scheme for O_2 evolution in PSII, in Photosynthesis: Energy from the Sun, ed. by Allen J. F., Gantt, E., Golbeck, J. H., Osmond, B., Springer (2008) 113-116.

[9] A. Zouni, H.T. Witt, J. Kern, P. Fromme, N. Krauss, W. Saenger and P. Orth, Crystal structure of photosystem II from *Synechococcus elongatus* at 3.8 Å resolution, Nature 409 (2001) 739-743.

[10] F. Rappaport, M. Guergova-Kuras, P.J. Nixon, B.A. Diner and J. Lavergne, Kinetics and pathways of charge recombination in photosystem II, Biochemistry 41 (2002) 8518-8527.

[11] A. Krieger, A.W. Rutherford and G.N. Johnson, On the determination of redox midpoint potential of the primary quinone electron transfer acceptor, Q_A, in photosystem II, Biochim. Biophys. Acta 1229 (1995) 193-201.

[12] G.N. Johnson, A.W. Rutherford and A. Krieger, A change in the midpoint potential of the quinone Q_A in Photosystem II associated with photoactivation of oxygen evolution, Biochim. Biophys. Acta 1229 (1995) 202-207.

[13] M. Grabolle and H. Dau, Energetics of primary and secondary electron transfer in Photosystem II membrane particles of spinach revisited on basis of recombination-fluorescence measurements, Biochim. Biophys. Acta 1708 (2005) 209-218.

[14] B. Loll, J. Kern, W. Saenger, A. Zouni and J. Biesiadka, Towards complete cofactor arrangement in the 3.0 Å resolution structure of photosystem II, Nature 438 (2005) 1040-1044.

[15] H. Ishikita, W. Saenger, J. Biesiadka, B. Loll and E.-W. Knapp, How photosynthetic reaction centers control oxidation power in chlorophyll pairs P680, P700 and P870, Proc. Natl. Acad. Sci. USA 103 (2006) 9855-9860.

[16] Y. Kato, M. Sugiura, A. Oda and T. Watanabe, Spectroelectrochemical determination of the redox potential of pheophytin *a*, the primary electron acceptor in photosystem II, Proc Natl Acad Sci U S A 106 (2009) 17365-17370.

[17] G. Renger and A.R. Holzwarth, Plastoquinone Oxido-Reductase in Photosynthesis, in Photosystem II (eds Wydrqynski, T., Satoh, K.) Springer, Dordrecht, The Netherlands (2005) 139-175.

[18] G. Renger, in Primary Processes of Photosynthesis: Principles and Apparatus, Part II (ed Renger G) Royal Society Chemistry, Cambridge, UK (2008) 237-290.

[19] H. Dau and M. Haumann, The manganese complex of photosystem II in its reaction cycle? Basic framework and possible realization at the atomic level, Coord. Chem. Rev. 252 (2008) 273-295.

[20] F. Rappaport and B.A. Diner, Primary photochemistry and energetics leading to the oxidation of the Mn_4Ca cluster and to the evolution of molecular oxygen in photosystem II, Coord. Chem. Rev. 252 (2008) 259-272.

[21] S.E.J. Rigby, J.H.A. Nugent and P.J. O'Malley, ENDOR and special triple resonance studies of chlorophyll cation radicals in photosystem 2, Biochemistry 33 (1994) 10043-10050.

[22] B.A. Diner, E. Schlodder, P.J. Nixon, W.J. Coleman, F. Rappaport, J. Lavergne, W.F.J. Vermaas and D.A. Chisholm, Site-directed mutations at D1-His198 and D2-His197 of photosystem II in *Synechocystis* PCC 6803: sites of primary charge separation and cation and triplet stabilization, Biochemistry 40 (2001) 9265-9281.

[23] H. Michel and J. Deisenhofer, Relevance of the photosynthetic reaction center from purple bacteria to the structure of photosystem II, Biochemistry 27 (1988) 1-7.

[24] K. Saito, T. Ishida, M. Sugiura, K. Kawakami, Y. Umena, N. Kamiya, J.-R. Shen and H. Ishikita, Distribution of the cationic state over the chlorophyll pair of photosystem II reaction center, J. Am. Chem. Soc. 133 (2011) 14379-14388.

[25] K. Saito and H. Ishikita, Cationic state distribution over the P700 chlorophyll pair in Photosystem I, Biophys. J. 101 (2011) 2018-2025.

[26] M. Akiyama, H. Miyashita, H. Kise, T. Watanabe, M. Mimuro, S. Miyachi and M. Kobayashi, Quest for minor but key chlorophyll molecules in photosynthetic reaction centers - unusual pigment composition in the reaction centers of the chlorophyll *d*-dominated cyanobacterium *Acaryochloris marina*, Photosynth Res 74 (2002) 97-107.

[27] M. Mimuro, S. Akimoto, T. Gotoh, M. Yokono, M. Akiyama, T. Tsuchiya, H. Miyashita, M. Kobayashi and I. Yamazaki, Identification of the primary electron donor in PS II of the Chl *d*-dominated cyanobacterium *Acaryochloris marina*, FEBS Lett 556 (2004) 95-8.

[28] M. Chen, A. Telfer, S. Lin, A. Pascal, A.W. Larkum, J. Barber and R.E. Blankenship, The nature of the photosystem II reaction centre in the chlorophyll *d*-containing prokaryote, *Acaryochloris marina*, Photochem Photobiol Sci 4 (2005) 1060-4.

[29] W.D. Swingley, M.F. Hohmann-Marriott, T. Le Olson and R.E. Blankenship, Effect of iron on growth and ultrastructure of Acaryochloris marina, Appl Environ Microbiol 71 (2005) 8606-10.

[30] S.I. Allakhverdiev, T. Tomo, Y. Shimada, H. Kindo, R. Nagao, V.V. Klimov and M. Mimuro, Redox potential of pheophytin a in photosystem II of two cyanobacteria having the different special pair chlorophylls, Proc Natl Acad Sci U S A 107 (2010) 3924-9.

[31] E. Schlodder, M. Cetin, H.J. Eckert, F.J. Schmitt, J. Barber and A. Telfer, Both chlorophylls *a* and *d* are essential for the photochemistry in photosystem II of the cyanobacteria, *Acaryochloris marina*, Biochim Biophys Acta 1767 (2007) 589-95.

[32] M. Sugiura, F. Rappaport, K. Brettel, T. Noguchi, A.W. Rutherford and A. Boussac, Site-directed mutagenesis of *Thermosynechococcus elongatus* photosystem II: the O_2-evolving enzyme lacking the redox-active tyrosine D, Biochemistry 43 (2004) 13549-13563.

[33] T. Okubo, T. Tomo, M. Sugiura and T. Noguchi, Perturbation of the structure of P680 and the charge distribution on its radical cation in isolated reaction center complexes of photosystem II as revealed by fourier transform infrared spectroscopy, Biochemistry 46 (2007) 4390-4397.

[34] T. Renger and E. Schlodder, The primary electron donor of photosystem II of the cyanobacterium *Acaryochloris marina* is a chlorophyll *d* and the water oxidation is driven by a chlorophyll *a*/chlorophyll *d* heterodimer, J Phys Chem B 112 (2008) 7351-4.

[35] K. Cser, Z. Deak, A. Telfer, J. Barber and I. Vass, Energetics of Photosystem II charge recombination in *Acaryochloris marina* studied by thermoluminescence and flash-induced chlorophyll fluorescence measurements, Photosynth Res 98 (2008) 131-40.

[36] T. Tomo, T. Okubo, S. Akimoto, M. Yokono, H. Miyashita, T. Tsuchiya, T. Noguchi and M. Mimuro, Identification of the special pair of photosystem II in a chlorophyll *d*-dominated cyanobacterium, Proc Natl Acad Sci U S A 104 (2007) 7283-8.

[37] T. Tomo, S.I. Allakhverdiev and M. Mimuro, Constitution and energetics of photosystem I and photosystem II in the chlorophyll d-dominated cyanobacterium *Acaryochloris marina*, J Photochem Photobiol B 104 (2011) 333-40.

[38] S.I. Allakhverdiev, T. Tsuchiya, K. Watabe, A. Kojima, D.A. Los, T. Tomo, V.V. Klimov and M. Mimuro, Redox potentials of primary electron acceptor quinone molecule $(Q_A)^-$ and conserved energetics of photosystem II in cyanobacteria with chlorophyll *a* and chlorophyll *d*, Proc Natl Acad Sci U S A 108 (2011) 8054-8.

[39] M. Kobayashi, S. Ohashi, K. Iwamoto, Y. Shiraiwa, Y. Kato and T. Watanabe, Redox potential of chlorophyll *d in vitro*, Biochim Biophys Acta 1767 (2007) 596-602.

[40] V. Sivakumar, R. Wang and G. Hastings, Photo-oxidation of P740, the primary electron donor in photosystem I from *Acaryochloris marina*, Biophys J 85 (2003) 3162-72.

[41] G. Hastings and R. Wang, Vibrational mode frequency calculations of chlorophyll-*d* for assessing ($P740^+$-P740) FTIR difference spectra obtained using photosystem I particles from *Acaryochloris marina*, Photosynth Res 95 (2008) 55-62.

[42] Y. Umena, K. Kawakami, J.-R. Shen and N. Kamiya, Crystal structure of oxygen-evolving photosystem II at 1.9 Å resolution, Nature 473 (2011) 55-60.

[43] M. Mimuro, S. Akimoto, I.I. Yamazaki, H. Miyashita and S. Miyachi, Fluorescence properties of chlorophyll *d*-dominating prokaryotic alga, *acaryochloris marina*: studies using time-resolved fluorescence spectroscopy on intact cells, Biochim Biophys Acta 1412 (1999) 37-46.

[44] B.R. Brooks, R.E. Bruccoleri, B.D. Olafson, D.J. States, S. Swaminathan and M. Karplus, CHARMM: a program for macromolecular energy minimization and dynamics calculations, J. Comput. Chem. 4 (1983) 187-217.

[45] A.D. MacKerell, Jr., D. Bashford, R.L. Bellott, R.L. Dunbrack, Jr., J.D. Evanseck, M.J. Field, S. Fischer, J. Gao, H. Guo, S. Ha, D. Joseph-McCarthy, L. Kuchnir, K. Kuczera, F.T.K. Lau, C. Mattos, S. Michnick, T. Ngo, D.T. Nguyen, B. Prodhom, W.E. Reiher, III, B. Roux, M. Schlenkrich, J.C. Smith, R. Stote, J. Straub, M. Watanabe, J. Wiorkiewicz-Kuczera, D. Yin and M. Karplus, All-atom empirical potential for molecular modeling and dynamics studies of proteins, J. Phys. Chem. B 102 (1998) 3586-3616.

[46] B. Rabenstein, G.M. Ullmann and E.-W. Knapp, Calculation of protonation patterns in proteins with structural relaxation and molecular ensembles - application to the photosynthetic reaction center, Eur. Biophys. J. 27 (1998) 626-637.

[47] K. Kanda, S. Yamanaka, T. Saito, Y. Umena, K. Kawakami, J.-R. Shen, N. Kamiya, M. Okumura, H. Nakamura and K. Yamaguchi, Labile electronic and spin states of the $CaMn_4O_5$ cluster in the PSII system refined to the 1.9 Å X-ray resolution. UB3LYP computational results, Chem. Phys. Lett. 506 (2011) 98-103.

[48] S. Luber, I. Rivalta, Y. Umena, K. Kawakami, J.-R. Shen, N. Kamiya, G.W. Brudvig and V.S. Batista, S_1-state model of the O_2-evolving complex of photosystem II, Biochemistry 50 (2011) 6308-6311.

[49] QSite, version 5.6, Schrödinger, LLC, New York, NY, 2010.

[50] Y. Li, M.-G. Lucas, T. Konovalova, B. Abbott, F. MacMillan, A. Petrenko, V. Sivakumar, R. Wang, G. Hastings, F. Gu, J. van Tol, L.-C. Brunel, R. Timkovich, F. Rappaport and K. Redding, Mutation of the putative hydrogen-bond donor to P_{700} of photosystem I, Biochemistry 43 (2004) 12634-12647.

[51] F. Muh, F. Lendzian, M. Roy, J.C. Williams, J.P. Allen and W. Lubitz, Pigment-protein interactions in bacterial reaction centers and their influence on oxidation potential and spin density distribution of the primary donor, J. Phys. Chem. B 106 (2002) 3226-3236.

[52] H. Witt, E. Schlodder, C. Teutloff, J. Niklas, E. Bordignon, D. Carbonera, S. Kohler, A. Labahn and W. Lubitz, Hydrogen bonding to P700: site-directed mutagenesis of threonine A739 of photosystem I in *Chlamydomonas reinhardtii*, Biochemistry 41 (2002) 8557-8569.

FIGURE CAPTIONS

FIGURE 1: Structure of (a) Chl*d* and (b) Chl*a* using the IUPAC numbering scheme (R = phytol chain).

FIGURE 2: Possible orientations of the formyl group in Chl*d*; (a) one with the carbonyl O atom being oriented to the C5 H atom and (b) another one with the formyl group flipped along the C3-$C3^1$ axis.

(a)

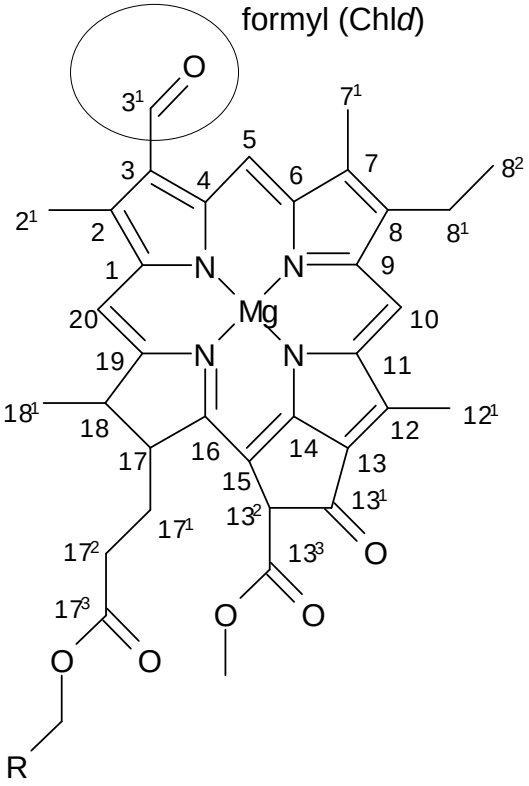
formyl (Chl*d*)
O
3^1
7^1
5
3
4
6
7
8^2
2^1
2
8
8^1
1
N
N
9
Mg
20
10
19
N
N
11
18^1
18
12^1
12
17
16
14
13
15
13^1
13^2
17^1
17^2
13^3
O
17^3
O
O
O
O
R

(b)

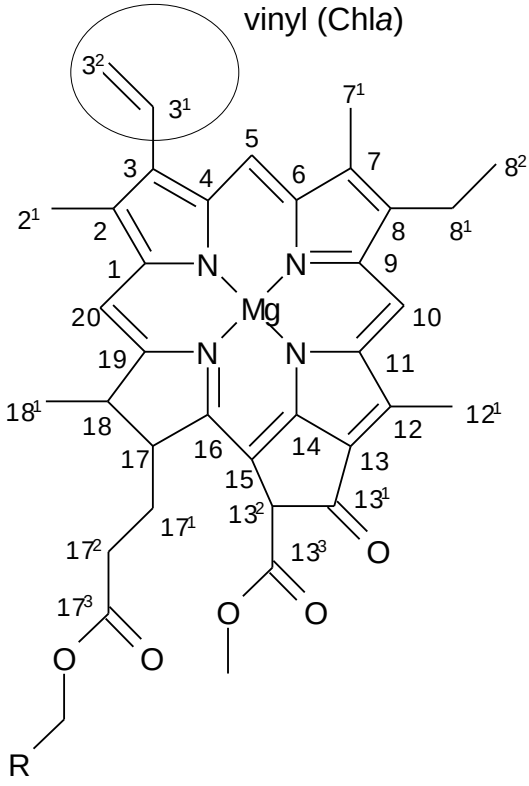
vinyl (Chl*a*)
3^2
3^1
7^1
5
3
4
6
7
8^2
2^1
2
8
8^1
1
N
N
9
Mg
20
10
19
N
N
11
18^1
18
12^1
12
17
16
14
13
15
13^1
13^2
17^1
17^2
13^3
O
17^3
O
O
O
O
R

FIGURE 1

(a)

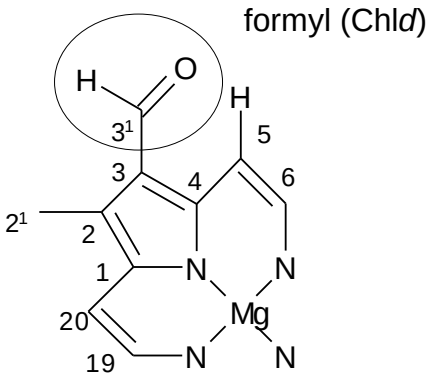
formyl (Chl*d*)
H
O
H
3¹
5
3
4
6
2¹
2
1
N
N
Mg
20
19
N
N

(b)

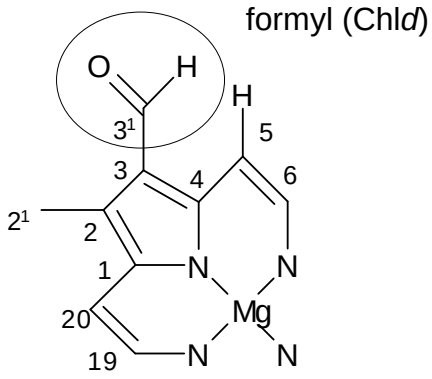
formyl (Chl*d*)
O
H
H
3¹
5
3
4
6
2¹
2
1
N
N
Mg
20
19
N
N

FIGURE 2

TABLE 1. Calculated values (%) for the $P_{D1}^{\bullet+}/P_{D2}^{\bullet+}$ ratio and spin density distribution in the D1/D2 subunit of the *Thermosynechococcus vulcanus* PSII [42].

	charge		**spin**	
	$\mathbf{P_{D1}^{\bullet+}}$	$\mathbf{P_{D2}^{\bullet+}}$	$\mathbf{P_{D1}}$	$\mathbf{P_{D2}}$
[whole PSII]				
Chl*a*/Chl*a* (*T. vulcanus*[a])	76.9	23.1	80.1	19.9
Chl*d*/Chl*d* (Tomo et al.[b])	76.5	23.5	85.1	14.9
Chl*a*/Chl*d* (Schlodder et al.[c])	85.1	14.9	95.2	4.8
Chl*d*/Chl*a*	56.7	43.3	55.8	44.2

[a] See Ref. [24].

[b] See Refs. [36, 37].

[c] See Ref. [31].

Cationic state distribution over the chlorophyll *d* -containing P_{D1}/P_{D2} pair in photosystem II

Keisuke Saito, Jian-Ren Shen, and Hiroshi Ishikita

Table S1. Atomic charges (**ESP: unrestricted DFT**) summarized in Table 1 in the main text and atomic coordinates.

(a) Chl*a*/Chl*a* (*T. vulcanus*)

atom	x	y	z	charge
PD1 MG	-19.914	-45.136	189.572	1.5528
PD1 CHA	-23.352	-44.836	188.885	-0.1854
PD1 CHB	-19.556	-46.569	186.476	-0.497
PD1 HHB	-19.428	-47.128	185.559	0.1628
PD1 CHC	-16.545	-44.432	189.617	-0.4855
PD1 HHC	-15.478	-44.254	189.665	0.1941
PD1 CHD	-20.349	-42.887	192.209	-0.5775
PD1 HHD	-20.478	-42.246	193.076	0.2548
PD1 NA	-21.283	-45.601	187.915	-0.5933
PD1 C1A	-22.65	-45.406	187.854	0.1961
PD1 C2A	-23.201	-45.815	186.503	0.0071
PD1 H2A	-24.15	-46.348	186.614	0.0652
PD1 C3A	-22.073	-46.733	185.991	0.0761
PD1 H3A	-21.883	-46.589	184.922	0.0253
PD1 C4A	-20.882	-46.272	186.824	0.433
PD1 CMA	-22.35	-48.216	186.273	-0.3975
PD1 HMA1	-23.241	-48.561	185.738	0.0977
PD1 HMA2	-22.508	-48.382	187.344	0.1247
PD1 HMA3	-21.498	-48.822	185.957	0.1074
PD1 CAA	-23.421	-44.569	185.606	0.2187
PD1 HAA1	-22.443	-44.148	185.355	-0.011
PD1 HAA2	-23.963	-43.802	186.166	0.021
PD1 CBA	-24.185	-44.844	184.31	-0.6022
PD1 HBA1	-23.743	-45.663	183.73	0.131
PD1 HBA2	-24.137	-43.961	183.661	0.173
PD1 CGA	-25.652	-45.156	184.538	0.7933
PD1 O1A	-26.229	-45.085	185.603	-0.4926
PD1 O2A	-26.251	-45.522	183.387	-0.3732
PD1 NB	-18.327	-45.45	188.28	-0.8152
PD1 C1B	-18.379	-46.161	187.108	0.3582

PD1	C2B	-17.035	-46.376	186.589	0.1782
PD1	C3B	-16.175	-45.721	187.446	-0.2492
PD1	C4B	-17.013	-45.169	188.517	0.5507
PD1	CMB	-16.7	-47.185	185.385	-0.4232
PD1	HMB1	-17.547	-47.781	185.038	0.1085
PD1	HMB2	-15.886	-47.877	185.619	0.148
PD1	HMB3	-16.369	-46.554	184.552	0.1357
PD1	CAB	-14.738	-45.517	187.374	0.0241
PD1	HAB	-14.286	-45.054	188.245	0.0778
PD1	CBB	-13.918	-45.781	186.344	-0.3733
PD1	HBB1	-12.865	-45.536	186.408	0.1549
PD1	HBB2	-14.27	-46.173	185.4	0.1455
PD1	NC	-18.661	-43.935	190.761	-0.8154
PD1	C1C	-17.298	-43.835	190.626	0.4223
PD1	C2C	-16.749	-42.961	191.654	0.0627
PD1	C3C	-17.809	-42.527	192.406	-0.2599
PD1	C4C	-19.007	-43.147	191.82	0.6294
PD1	CMC	-15.301	-42.627	191.827	-0.1977
PD1	HMC1	-14.837	-42.345	190.877	0.0167
PD1	HMC2	-14.744	-43.469	192.238	0.0816
PD1	HMC3	-15.159	-41.803	192.524	0.1185
PD1	CAC	-17.715	-41.622	193.598	0.0318
PD1	HAC1	-17.066	-42.12	194.329	0.0802
PD1	HAC2	-18.694	-41.534	194.068	0.0414
PD1	CBC	-17.158	-40.207	193.341	-0.1367
PD1	HBC1	-16.245	-40.215	192.743	0.0112
PD1	HBC2	-16.912	-39.738	194.296	0.0895
PD1	HBC3	-17.871	-39.562	192.825	0.0476
PD1	ND	-21.467	-44.114	190.415	-0.9155
PD1	C1D	-21.501	-43.294	191.539	0.5764
PD1	C2D	-22.897	-42.907	191.822	0.0489
PD1	C3D	-23.637	-43.51	190.829	-0.2908
PD1	C4D	-22.731	-44.239	190.011	0.5059
PD1	CMD	-23.374	-42.105	192.97	-0.4552
PD1	HMD1	-22.53	-41.85	193.602	0.1331
PD1	HMD2	-24.094	-42.672	193.568	0.1947

PD1	HMD3	-23.885	-41.187	192.66	0.1751
PD1	CAD	-24.972	-43.554	190.231	0.6954
PD1	OBD	-25.979	-42.96	190.547	-0.459
PD1	CBD	-24.829	-44.466	188.933	-0.6753
PD1	HBD1	-25.157	-43.882	188.068	0.1997
PD1	CGD	-25.848	-45.557	189.042	0.8822
PD1	O1D	-25.66	-46.646	189.54	-0.5914
PD1	O2D	-27.022	-45.099	188.608	-0.3265
PD1	CED	-28.158	-45.94	188.828	-0.154
PD1	HED1	-28.053	-46.468	189.775	0.1097
PD1	HED2	-28.244	-46.665	188.015	0.1201
PD1	HED3	-29.017	-45.269	188.85	0.124
PD1	C1	-27.644	-45.876	183.518	-0.1068
PD1	H1	-27.763	-46.629	184.292	0.1241
PD1	H2	-27.933	-46.264	182.54	0.0986
PD1	H3	-28.233	-44.99	183.765	0.0932
PD2	MG	-13.534	-42.66	185.027	1.3137
PD2	CHA	-10.514	-44.017	183.826	0.0966
PD2	CHB	-15.145	-44.492	182.583	-0.4322
PD2	HHB	-15.684	-44.965	181.767	0.1497
PD2	CHC	-16.483	-42.158	186.638	-0.186
PD2	HHC	-17.434	-41.882	187.078	0.1463
PD2	CHD	-11.836	-41.675	187.893	-0.5191
PD2	HHD	-11.296	-41.27	188.743	0.2203
PD2	NA	-12.884	-43.982	183.384	-0.2896
PD2	C1A	-11.608	-44.346	183.052	-0.1944
PD2	C2A	-11.569	-45.224	181.821	0.1677
PD2	H2A	-10.831	-44.849	181.098	-0.0054
PD2	C3A	-13.005	-45.08	181.286	0.3488
PD2	H3A	-13.398	-46.061	181.019	-0.0549
PD2	C4A	-13.761	-44.494	182.477	0.0699
PD2	CMA	-13.083	-44.142	180.081	-0.4287
PD2	HMA1	-12.495	-44.523	179.238	0.0782
PD2	HMA2	-12.707	-43.151	180.354	0.1006
PD2	HMA3	-14.117	-44.033	179.758	0.1242

PD2	CAA	-11.203	-46.676	182.169	0.1725
PD2	HAA1	-11.949	-47.06	182.871	0.0162
PD2	HAA2	-10.241	-46.718	182.683	-0.0009
PD2	CBA	-11.139	-47.582	180.932	-0.6793
PD2	HBA1	-10.305	-47.264	180.299	0.1596
PD2	HBA2	-12.057	-47.534	180.344	0.1557
PD2	CGA	-10.948	-49.024	181.33	0.8471
PD2	O1A	-11.75	-49.91	181.133	-0.5501
PD2	O2A	-9.776	-49.191	181.965	-0.3426
PD2	NB	-15.472	-43.261	184.682	-0.4856
PD2	C1B	-15.948	-43.965	183.628	0.2495
PD2	C2B	-17.404	-44.078	183.719	0.0474
PD2	C3B	-17.778	-43.399	184.858	0.0281
PD2	C4B	-16.547	-42.901	185.467	0.0701
PD2	CMB	-18.282	-44.844	182.784	-0.2918
PD2	HMB1	-17.972	-45.893	182.71	0.0682
PD2	HMB2	-18.276	-44.434	181.767	0.091
PD2	HMB3	-19.309	-44.819	183.151	0.0826
PD2	CAB	-19.097	-43.183	185.469	-0.0857
PD2	HAB	-19.164	-43.428	186.528	0.0651
PD2	CBB	-20.172	-42.65	184.876	-0.3394
PD2	HBB1	-21.087	-42.466	185.428	0.1386
PD2	HBB2	-20.157	-42.321	183.845	0.1585
PD2	NC	-14.068	-42.065	186.974	-0.5127
PD2	C1C	-15.33	-41.721	187.331	0.1054
PD2	C2C	-15.31	-40.844	188.496	0.1423
PD2	C3C	-13.987	-40.685	188.84	-0.2318
PD2	C4C	-13.222	-41.48	187.887	0.4202
PD2	CMC	-16.511	-40.231	189.141	-0.3928
PD2	HMC1	-17.044	-40.965	189.757	0.0928
PD2	HMC2	-17.213	-39.835	188.399	0.1003
PD2	HMC3	-16.237	-39.406	189.802	0.1625
PD2	CAC	-13.421	-39.779	189.895	0.2326
PD2	HAC1	-12.967	-40.358	190.707	0.0146
PD2	HAC2	-14.244	-39.226	190.357	0.0192
PD2	CBC	-12.39	-38.777	189.336	-0.387

PD2	HBC1	-11.372	-39.166	189.425	0.085
PD2	HBC2	-12.427	-37.833	189.879	0.1314
PD2	HBC3	-12.591	-38.554	188.283	0.0874
PD2	ND	-11.632	-42.845	185.757	-0.6268
PD2	C1D	-11.075	-42.359	186.929	0.3685
PD2	C2D	-9.636	-42.609	186.941	0.1057
PD2	C3D	-9.37	-43.204	185.723	-0.3057
PD2	C4D	-10.612	-43.346	185.052	0.1883
PD2	CMD	-8.68	-42.299	188.027	-0.3834
PD2	HMD1	-8.634	-43.092	188.78	0.1418
PD2	HMD2	-9.006	-41.399	188.533	0.1147
PD2	HMD3	-7.67	-42.155	187.641	0.1588
PD2	CAD	-8.31	-43.768	184.901	0.7241
PD2	OBD	-7.116	-43.84	185.103	-0.4812
PD2	CBD	-9.036	-44.334	183.601	-0.6943
PD2	HBD1	-8.806	-45.398	183.509	0.2002
PD2	CGD	-8.453	-43.607	182.414	0.8375
PD2	O1D	-8.618	-42.423	182.235	-0.5543
PD2	O2D	-7.711	-44.394	181.632	-0.3656
PD2	CED	-6.933	-43.722	180.616	-0.1001
PD2	HED1	-6.681	-42.715	180.935	0.1211
PD2	HED2	-7.494	-43.671	179.686	0.105
PD2	HED3	-6.037	-44.318	180.474	0.1165
PD2	C1	-9.498	-50.523	182.417	-0.1022
PD2	H1	-9.685	-51.247	181.623	0.083
PD2	H2	-10.114	-50.757	183.286	0.1152
PD2	H3	-8.446	-50.527	182.698	0.1139

total (PD1)	0.7694
total (PD2)	0.2306

(b) Chl*d*/Chl*d* (Tomo et al.)

atom	x	y	z	charge
PD1 MG	-19.911	-45.135	189.566	1.5752
PD1 CHA	-23.351	-44.836	188.885	-0.1753
PD1 CHB	-19.557	-46.571	186.476	-0.5763
PD1 HHB	-19.431	-47.129	185.558	0.1701
PD1 CHC	-16.537	-44.425	189.612	-0.5181
PD1 HHC	-15.468	-44.255	189.66	0.2029
PD1 CHD	-20.347	-42.89	192.206	-0.5804
PD1 HHD	-20.474	-42.251	193.074	0.2549
PD1 NA	-21.282	-45.602	187.914	-0.7294
PD1 C1A	-22.65	-45.404	187.852	0.2914
PD1 C2A	-23.201	-45.807	186.502	-0.1549
PD1 H2A	-24.15	-46.341	186.614	0.09
PD1 C3A	-22.073	-46.726	185.988	0.1293
PD1 H3A	-21.879	-46.576	184.921	0.0164
PD1 C4A	-20.887	-46.27	186.823	0.5886
PD1 CMA	-22.349	-48.211	186.269	-0.4354
PD1 HMA1	-23.24	-48.556	185.734	0.1098
PD1 HMA2	-22.509	-48.379	187.34	0.1292
PD1 HMA3	-21.499	-48.818	185.953	0.1105
PD1 CAA	-23.42	-44.555	185.61	0.4236
PD1 HAA1	-22.446	-44.119	185.365	-0.0997
PD1 HAA2	-23.977	-43.801	186.172	-0.0317
PD1 CBA	-24.184	-44.838	184.314	-0.5903
PD1 HBA1	-23.737	-45.655	183.734	0.1244
PD1 HBA2	-24.137	-43.956	183.665	0.1716
PD1 CGA	-25.65	-45.156	184.54	0.7619
PD1 O1A	-26.23	-45.091	185.605	-0.4912
PD1 O2A	-26.25	-45.523	183.389	-0.3698
PD1 NB	-18.316	-45.446	188.273	-0.8135
PD1 C1B	-18.382	-46.161	187.102	0.4089
PD1 C2B	-17.04	-46.383	186.578	0.2537
PD1 C3B	-16.182	-45.721	187.437	-0.3889
PD1 C4B	-17.006	-45.162	188.504	0.5477

PD1	CMB	-16.683	-47.182	185.377	-0.5319
PD1	HMB1	-17.545	-47.703	184.955	0.1286
PD1	HMB2	-15.923	-47.919	185.64	0.1928
PD1	HMB3	-16.238	-46.546	184.605	0.1792
PD1	CAB	-14.738	-45.545	187.271	0.5371
PD1	HAB	-14.24	-44.898	188.018	-0.0479
PD1	OAB	-14.074	-46.048	186.373	-0.4787
PD1	NC	-18.657	-43.935	190.755	-0.8445
PD1	C1C	-17.289	-43.835	190.62	0.4563
PD1	C2C	-16.743	-42.962	191.651	0.0566
PD1	C3C	-17.804	-42.529	192.401	-0.258
PD1	C4C	-19.001	-43.151	191.813	0.6494
PD1	CMC	-15.294	-42.631	191.826	-0.2099
PD1	HMC1	-14.81	-42.428	190.866	0.0251
PD1	HMC2	-14.754	-43.443	192.314	0.0894
PD1	HMC3	-15.155	-41.755	192.456	0.1204
PD1	CAC	-17.714	-41.624	193.595	0.0265
PD1	HAC1	-17.065	-42.122	194.326	0.0829
PD1	HAC2	-18.694	-41.538	194.065	0.0416
PD1	CBC	-17.159	-40.207	193.342	-0.128
PD1	HBC1	-16.248	-40.211	192.741	0.0088
PD1	HBC2	-16.912	-39.742	194.298	0.0883
PD1	HBC3	-17.875	-39.561	192.831	0.0466
PD1	ND	-21.465	-44.115	190.413	-0.9083
PD1	C1D	-21.497	-43.295	191.537	0.573
PD1	C2D	-22.896	-42.908	191.821	0.0617
PD1	C3D	-23.635	-43.509	190.829	-0.3047
PD1	C4D	-22.728	-44.239	190.01	0.5178
PD1	CMD	-23.373	-42.106	192.97	-0.4624
PD1	HMD1	-22.529	-41.851	193.602	0.1358
PD1	HMD2	-24.093	-42.674	193.567	0.1967
PD1	HMD3	-23.884	-41.189	192.659	0.1785
PD1	CAD	-24.97	-43.554	190.229	0.714
PD1	OBD	-25.976	-42.959	190.548	-0.459
PD1	CBD	-24.828	-44.465	188.933	-0.7062
PD1	HBD1	-25.154	-43.883	188.066	0.2158

PD1	CGD	-25.847	-45.556	189.042	0.8808
PD1	O1D	-25.656	-46.645	189.54	-0.5907
PD1	O2D	-27.02	-45.098	188.61	-0.3261
PD1	CED	-28.157	-45.94	188.827	-0.1481
PD1	HED1	-28.052	-46.472	189.772	0.1084
PD1	HED2	-28.243	-46.662	188.011	0.1197
PD1	HED3	-29.015	-45.269	188.852	0.1231
PD1	C1	-27.644	-45.876	183.518	-0.0984
PD1	H1	-27.762	-46.652	184.27	0.1215
PD1	H2	-27.941	-46.233	182.531	0.0946
PD1	H3	-28.228	-44.996	183.796	0.0919
PD2	MG	-13.536	-42.673	185.026	1.3921
PD2	CHA	-10.514	-44.013	183.829	0.0322
PD2	CHB	-15.136	-44.495	182.582	-0.5151
PD2	HHB	-15.677	-44.969	181.769	0.1576
PD2	CHC	-16.497	-42.153	186.644	-0.2646
PD2	HHC	-17.438	-41.863	187.095	0.1829
PD2	CHD	-11.84	-41.678	187.89	-0.6306
PD2	HHD	-11.302	-41.271	188.74	0.23
PD2	NA	-12.881	-43.98	183.383	-0.4067
PD2	C1A	-11.612	-44.344	183.053	-0.0608
PD2	C2A	-11.567	-45.223	181.822	0.1133
PD2	H2A	-10.828	-44.847	181.103	0.0046
PD2	C3A	-13.002	-45.079	181.284	0.3277
PD2	H3A	-13.395	-46.061	181.018	-0.0512
PD2	C4A	-13.757	-44.494	182.473	0.1967
PD2	CMA	-13.081	-44.142	180.078	-0.4352
PD2	HMA1	-12.492	-44.522	179.236	0.0839
PD2	HMA2	-12.706	-43.15	180.351	0.0973
PD2	HMA3	-14.114	-44.034	179.755	0.126
PD2	CAA	-11.204	-46.675	182.172	0.1893
PD2	HAA1	-11.949	-47.058	182.875	0.0272
PD2	HAA2	-10.241	-46.718	182.686	-0.0028
PD2	CBA	-11.14	-47.58	180.935	-0.6993
PD2	HBA1	-10.306	-47.263	180.3	0.1642

PD2	HBA2	-12.058	-47.533	180.346	0.1628
PD2	CGA	-10.948	-49.023	181.33	0.85
PD2	O1A	-11.749	-49.91	181.131	-0.5501
PD2	O2A	-9.776	-49.191	181.965	-0.3425
PD2	NB	-15.492	-43.266	184.698	-0.5314
PD2	C1B	-15.947	-43.981	183.629	0.3147
PD2	C2B	-17.383	-44.113	183.698	0.132
PD2	C3B	-17.784	-43.426	184.839	-0.2402
PD2	C4B	-16.572	-42.904	185.463	0.1668
PD2	CMB	-18.261	-44.859	182.749	-0.333
PD2	HMB1	-18.037	-45.932	182.764	0.0777
PD2	HMB2	-18.138	-44.514	181.717	0.0971
PD2	HMB3	-19.297	-44.714	183.042	0.1054
PD2	CAB	-19.138	-43.243	185.342	0.4618
PD2	HAB	-19.217	-42.672	186.289	-0.072
PD2	OAB	-20.167	-43.656	184.815	-0.3985
PD2	NC	-14.076	-42.082	186.979	-0.5726
PD2	C1C	-15.344	-41.728	187.332	0.1063
PD2	C2C	-15.317	-40.846	188.496	0.1641
PD2	C3C	-13.993	-40.691	188.837	-0.3073
PD2	C4C	-13.232	-41.493	187.884	0.5727
PD2	CMC	-16.514	-40.228	189.143	-0.3842
PD2	HMC1	-17.042	-40.957	189.767	0.0846
PD2	HMC2	-17.219	-39.838	188.401	0.0992
PD2	HMC3	-16.237	-39.397	189.795	0.1632
PD2	CAC	-13.423	-39.783	189.891	0.252
PD2	HAC1	-12.968	-40.362	190.702	0.0122
PD2	HAC2	-14.245	-39.229	190.353	0.0185
PD2	CBC	-12.391	-38.78	189.334	-0.3903
PD2	HBC1	-11.373	-39.169	189.424	0.087
PD2	HBC2	-12.43	-37.837	189.878	0.1326
PD2	HBC3	-12.591	-38.556	188.281	0.0872
PD2	ND	-11.636	-42.841	185.756	-0.8411
PD2	C1D	-11.081	-42.356	186.927	0.5459
PD2	C2D	-9.635	-42.607	186.939	0.0498
PD2	C3D	-9.372	-43.201	185.724	-0.3145

PD2	C4D	-10.616	-43.344	185.051	0.3414
PD2	CMD	-8.681	-42.298	188.026	-0.3612
PD2	HMD1	-8.639	-43.092	188.778	0.1424
PD2	HMD2	-9.005	-41.397	188.531	0.1091
PD2	HMD3	-7.67	-42.157	187.641	0.1569
PD2	CAD	-8.312	-43.768	184.9	0.7453
PD2	OBD	-7.118	-43.837	185.104	-0.4785
PD2	CBD	-9.038	-44.332	183.602	-0.7352
PD2	HBD1	-8.811	-45.398	183.511	0.2163
PD2	CGD	-8.453	-43.607	182.414	0.8322
PD2	O1D	-8.619	-42.422	182.237	-0.5531
PD2	O2D	-7.713	-44.394	181.633	-0.3591
PD2	CED	-6.933	-43.723	180.616	-0.0992
PD2	HED1	-6.681	-42.716	180.936	0.1219
PD2	HED2	-7.494	-43.672	179.687	0.1051
PD2	HED3	-6.038	-44.32	180.476	0.1159
PD2	C1	-9.498	-50.523	182.417	-0.1049
PD2	H1	-9.685	-51.247	181.623	0.0829
PD2	H2	-10.114	-50.756	183.286	0.1182
PD2	H3	-8.446	-50.527	182.699	0.1137

total (PD1)	0.7653
total (PD2)	0.2347

(c) Chl*a*/Chl*d* (Schlodder et al.)

atom	x	y	z	charge
PD1 MG	-19.928	-45.135	189.566	1.5793
PD1 CHA	-23.364	-44.825	188.889	-0.1795
PD1 CHB	-19.578	-46.571	186.477	-0.6221
PD1 HHB	-19.455	-47.126	185.556	0.1789
PD1 CHC	-16.56	-44.429	189.601	-0.511
PD1 HHC	-15.494	-44.249	189.639	0.2003
PD1 CHD	-20.354	-42.892	192.212	-0.5913
PD1 HHD	-20.479	-42.252	193.079	0.2563
PD1 NA	-21.297	-45.592	187.915	-0.7372
PD1 C1A	-22.664	-45.382	187.849	0.2848
PD1 C2A	-23.213	-45.766	186.495	-0.1272
PD1 H2A	-24.165	-46.294	186.601	0.0877
PD1 C3A	-22.092	-46.689	185.974	0.1111
PD1 H3A	-21.888	-46.529	184.91	0.0201
PD1 C4A	-20.905	-46.256	186.821	0.6227
PD1 CMA	-22.389	-48.174	186.24	-0.4415
PD1 HMA1	-23.283	-48.498	185.697	0.1114
PD1 HMA2	-22.559	-48.348	187.308	0.1296
PD1 HMA3	-21.548	-48.794	185.923	0.1134
PD1 CAA	-23.431	-44.503	185.614	0.3873
PD1 HAA1	-22.457	-44.068	185.365	-0.0873
PD1 HAA2	-23.983	-43.753	186.186	-0.0225
PD1 CBA	-24.202	-44.773	184.319	-0.5896
PD1 HBA1	-23.74	-45.564	183.716	0.1271
PD1 HBA2	-24.181	-43.874	183.691	0.1733
PD1 CGA	-25.659	-45.132	184.546	0.7623
PD1 O1A	-26.234	-45.101	185.616	-0.4898
PD1 O2A	-26.257	-45.494	183.392	-0.3708
PD1 NB	-18.346	-45.441	188.27	-0.8763
PD1 C1B	-18.405	-46.163	187.101	0.4814
PD1 C2B	-17.061	-46.39	186.582	0.1231
PD1 C3B	-16.2	-45.728	187.429	-0.2308
PD1 C4B	-17.038	-45.166	188.5	0.5811

PD1	CMB	-16.733	-47.22	185.39	-0.4188
PD1	HMB1	-17.575	-47.844	185.08	0.1119
PD1	HMB2	-15.897	-47.885	185.622	0.1498
PD1	HMB3	-16.44	-46.605	184.532	0.138
PD1	CAB	-14.761	-45.538	187.357	0.0171
PD1	HAB	-14.299	-45.101	188.236	0.0758
PD1	CBB	-13.953	-45.787	186.314	-0.3608
PD1	HBB1	-12.895	-45.561	186.376	0.1527
PD1	HBB2	-14.318	-46.15	185.363	0.1426
PD1	NC	-18.671	-43.938	190.756	-0.8372
PD1	C1C	-17.305	-43.836	190.614	0.4458
PD1	C2C	-16.752	-42.963	191.643	0.0604
PD1	C3C	-17.808	-42.532	192.399	-0.2621
PD1	C4C	-19.01	-43.153	191.815	0.655
PD1	CMC	-15.302	-42.631	191.808	-0.1942
PD1	HMC1	-14.835	-42.382	190.85	0.016
PD1	HMC2	-14.751	-43.463	192.248	0.0825
PD1	HMC3	-15.157	-41.785	192.477	0.1175
PD1	CAC	-17.715	-41.632	193.595	0.0319
PD1	HAC1	-17.067	-42.134	194.324	0.0809
PD1	HAC2	-18.695	-41.546	194.065	0.041
PD1	CBC	-17.158	-40.215	193.346	-0.1343
PD1	HBC1	-16.244	-40.219	192.75	0.0126
PD1	HBC2	-16.915	-39.751	194.304	0.0895
PD1	HBC3	-17.872	-39.568	192.832	0.0477
PD1	ND	-21.474	-44.116	190.419	-0.9108
PD1	C1D	-21.503	-43.296	191.542	0.581
PD1	C2D	-22.903	-42.905	191.827	0.0626
PD1	C3D	-23.644	-43.504	190.835	-0.3072
PD1	C4D	-22.739	-44.236	190.015	0.5195
PD1	CMD	-23.376	-42.103	192.976	-0.4613
PD1	HMD1	-22.528	-41.847	193.604	0.1351
PD1	HMD2	-24.092	-42.671	193.576	0.1966
PD1	HMD3	-23.888	-41.186	192.667	0.1784
PD1	CAD	-24.98	-43.544	190.236	0.7146
PD1	OBD	-25.984	-42.948	190.557	-0.4593

PD1	CBD	-24.84	-44.454	188.939	-0.7011
PD1	HBD1	-25.169	-43.871	188.074	0.2118
PD1	CGD	-25.854	-45.549	189.045	0.8793
PD1	O1D	-25.657	-46.642	189.532	-0.5899
PD1	O2D	-27.031	-45.091	188.622	-0.3264
PD1	CED	-28.161	-45.943	188.829	-0.1483
PD1	HED1	-28.054	-46.481	189.77	0.108
PD1	HED2	-28.241	-46.658	188.007	0.1196
PD1	HED3	-29.025	-45.278	188.857	0.1231
PD1	C1	-27.644	-45.876	183.518	-0.0979
PD1	H1	-27.75	-46.654	184.27	0.1208
PD1	H2	-27.931	-46.238	182.53	0.095
PD1	H3	-28.246	-45.008	183.795	0.0918
PD2	MG	-13.547	-42.676	184.99	1.3121
PD2	CHA	-10.502	-44.019	183.814	0.0825
PD2	CHB	-15.108	-44.507	182.519	-0.4556
PD2	HHB	-15.639	-44.978	181.698	0.1478
PD2	CHC	-16.523	-42.18	186.574	-0.2583
PD2	HHC	-17.472	-41.897	187.013	0.1794
PD2	CHD	-11.877	-41.689	187.86	-0.5087
PD2	HHD	-11.351	-41.278	188.716	0.2161
PD2	NA	-12.865	-43.987	183.344	-0.3182
PD2	C1A	-11.587	-44.347	183.026	-0.1619
PD2	C2A	-11.532	-45.224	181.795	0.1128
PD2	H2A	-10.779	-44.857	181.084	0.0077
PD2	C3A	-12.959	-45.076	181.237	0.376
PD2	H3A	-13.349	-46.055	180.959	-0.0583
PD2	C4A	-13.728	-44.498	182.422	0.0945
PD2	CMA	-13.021	-44.136	180.034	-0.4401
PD2	HMA1	-12.406	-44.504	179.205	0.0803
PD2	HMA2	-12.667	-43.14	180.322	0.1013
PD2	HMA3	-14.046	-44.04	179.684	0.127
PD2	CAA	-11.185	-46.677	182.153	0.1794
PD2	HAA1	-11.939	-47.051	182.851	0.016
PD2	HAA2	-10.225	-46.728	182.672	0.0007

PD2	CBA	-11.125	-47.587	180.919	-0.6802
PD2	HBA1	-10.287	-47.276	180.286	0.1606
PD2	HBA2	-12.041	-47.536	180.328	0.1573
PD2	CGA	-10.942	-49.027	181.323	0.8463
PD2	O1A	-11.749	-49.911	181.135	-0.5494
PD2	O2A	-9.77	-49.194	181.957	-0.3423
PD2	NB	-15.494	-43.277	184.63	-0.4674
PD2	C1B	-15.931	-43.997	183.558	0.241
PD2	C2B	-17.363	-44.143	183.612	0.1509
PD2	C3B	-17.785	-43.462	184.75	-0.2414
PD2	C4B	-16.585	-42.928	185.388	0.1409
PD2	CMB	-18.216	-44.887	182.639	-0.3219
PD2	HMB1	-17.977	-45.956	182.641	0.0713
PD2	HMB2	-18.078	-44.521	181.616	0.0947
PD2	HMB3	-19.259	-44.763	182.912	0.1004
PD2	CAB	-19.15	-43.296	185.227	0.4601
PD2	HAB	-19.26	-42.71	186.161	-0.0647
PD2	OAB	-20.162	-43.742	184.69	-0.4039
PD2	NC	-14.106	-42.097	186.932	-0.517
PD2	C1C	-15.379	-41.747	187.275	0.1222
PD2	C2C	-15.358	-40.866	188.439	0.1244
PD2	C3C	-14.036	-40.711	188.79	-0.2221
PD2	C4C	-13.271	-41.509	187.842	0.4152
PD2	CMC	-16.553	-40.244	189.087	-0.3938
PD2	HMC1	-17.077	-40.969	189.718	0.0896
PD2	HMC2	-17.26	-39.856	188.347	0.1021
PD2	HMC3	-16.271	-39.411	189.734	0.1635
PD2	CAC	-13.465	-39.815	189.855	0.2414
PD2	HAC1	-13.011	-40.406	190.659	0.0101
PD2	HAC2	-14.285	-39.266	190.324	0.0176
PD2	CBC	-12.426	-38.807	189.316	-0.3981
PD2	HBC1	-11.409	-39.197	189.41	0.0888
PD2	HBC2	-12.467	-37.871	189.873	0.134
PD2	HBC3	-12.616	-38.571	188.264	0.0907
PD2	ND	-11.648	-42.862	185.735	-0.6173
PD2	C1D	-11.104	-42.366	186.911	0.3537

PD2	C2D	-9.661	-42.605	186.935	0.1131
PD2	C3D	-9.382	-43.199	185.721	-0.3039
PD2	C4D	-10.618	-43.353	185.04	0.1941
PD2	CMD	-8.715	-42.287	188.029	-0.387
PD2	HMD1	-8.65	-43.093	188.766	0.1438
PD2	HMD2	-9.063	-41.404	188.55	0.1152
PD2	HMD3	-7.708	-42.115	187.647	0.1604
PD2	CAD	-8.31	-43.75	184.903	0.72
PD2	OBD	-7.115	-43.802	185.11	-0.4783
PD2	CBD	-9.022	-44.326	183.601	-0.6866
PD2	HBD1	-8.785	-45.391	183.516	0.1996
PD2	CGD	-8.439	-43.604	182.412	0.8341
PD2	O1D	-8.603	-42.419	182.23	-0.5524
PD2	O2D	-7.703	-44.394	181.629	-0.3643
PD2	CED	-6.925	-43.727	180.61	-0.1012
PD2	HED1	-6.667	-42.721	180.929	0.1218
PD2	HED2	-7.49	-43.672	179.683	0.1054
PD2	HED3	-6.033	-44.327	180.465	0.1166
PD2	C1	-9.498	-50.523	182.417	-0.1012
PD2	H1	-9.684	-51.252	181.627	0.0829
PD2	H2	-10.118	-50.751	183.285	0.1143
PD2	H3	-8.447	-50.53	182.704	0.1134

total (PD1)	0.8506
total (PD2)	0.1496

(d) Chl*d*/Chl*a*

atom	x	y	z	charge
PD1 MG	-19.911	-45.135	189.571	1.5483
PD1 CHA	-23.351	-44.835	188.885	-0.18
PD1 CHB	-19.561	-46.569	186.473	-0.4697
PD1 HHB	-19.431	-47.134	185.559	0.1545
PD1 CHC	-16.536	-44.43	189.615	-0.489
PD1 HHC	-15.468	-44.261	189.669	0.1947
PD1 CHD	-20.347	-42.887	192.208	-0.5677
PD1 HHD	-20.477	-42.247	193.075	0.253
PD1 NA	-21.284	-45.602	187.913	-0.5879
PD1 C1A	-22.647	-45.406	187.853	0.1955
PD1 C2A	-23.202	-45.816	186.502	-0.006
PD1 H2A	-24.151	-46.349	186.614	0.0672
PD1 C3A	-22.075	-46.735	185.989	0.0963
PD1 H3A	-21.887	-46.591	184.919	0.0191
PD1 C4A	-20.882	-46.274	186.818	0.4004
PD1 CMA	-22.351	-48.217	186.273	-0.3986
PD1 HMA1	-23.243	-48.563	185.739	0.0954
PD1 HMA2	-22.507	-48.382	187.344	0.1251
PD1 HMA3	-21.5	-48.822	185.956	0.1059
PD1 CAA	-23.422	-44.569	185.607	0.2045
PD1 HAA1	-22.444	-44.147	185.356	-0.0057
PD1 HAA2	-23.965	-43.803	186.167	0.0237
PD1 CBA	-24.186	-44.844	184.31	-0.5955
PD1 HBA1	-23.743	-45.663	183.731	0.1297
PD1 HBA2	-24.138	-43.961	183.661	0.17
PD1 CGA	-25.652	-45.156	184.538	0.7943
PD1 O1A	-26.23	-45.085	185.603	-0.4914
PD1 O2A	-26.251	-45.523	183.387	-0.3755
PD1 NB	-18.315	-45.45	188.275	-0.7503
PD1 C1B	-18.379	-46.163	187.107	0.2865
PD1 C2B	-17.044	-46.382	186.582	0.3232
PD1 C3B	-16.179	-45.723	187.444	-0.4322
PD1 C4B	-16.998	-45.167	188.511	0.5103

PD1	CMB	-16.693	-47.183	185.381	-0.5572
PD1	HMB1	-17.552	-47.734	184.99	0.1274
PD1	HMB2	-15.906	-47.897	185.631	0.1935
PD1	HMB3	-16.291	-46.545	184.587	0.1817
PD1	CAB	-14.737	-45.551	187.279	0.5557
PD1	HAB	-14.233	-44.932	188.046	-0.0525
PD1	OAB	-14.075	-46.029	186.365	-0.4945
PD1	NC	-18.657	-43.934	190.758	-0.8147
PD1	C1C	-17.293	-43.834	190.624	0.4128
PD1	C2C	-16.747	-42.962	191.652	0.0692
PD1	C3C	-17.809	-42.528	192.404	-0.258
PD1	C4C	-19.005	-43.147	191.819	0.6099
PD1	CMC	-15.299	-42.628	191.828	-0.2166
PD1	HMC1	-14.823	-42.389	190.871	0.0256
PD1	HMC2	-14.75	-43.455	192.28	0.0857
PD1	HMC3	-15.159	-41.775	192.489	0.1201
PD1	CAC	-17.715	-41.623	193.597	0.0279
PD1	HAC1	-17.066	-42.12	194.329	0.0811
PD1	HAC2	-18.694	-41.534	194.068	0.0422
PD1	CBC	-17.158	-40.207	193.341	-0.1359
PD1	HBC1	-16.246	-40.214	192.742	0.0077
PD1	HBC2	-16.912	-39.738	194.296	0.0888
PD1	HBC3	-17.873	-39.562	192.826	0.047
PD1	ND	-21.467	-44.114	190.414	-0.9129
PD1	C1D	-21.501	-43.293	191.539	0.566
PD1	C2D	-22.894	-42.907	191.822	0.041
PD1	C3D	-23.636	-43.51	190.828	-0.2854
PD1	C4D	-22.731	-44.239	190.01	0.4936
PD1	CMD	-23.374	-42.105	192.97	-0.4517
PD1	HMD1	-22.529	-41.851	193.602	0.1312
PD1	HMD2	-24.093	-42.673	193.567	0.1928
PD1	HMD3	-23.884	-41.187	192.66	0.172
PD1	CAD	-24.97	-43.553	190.231	0.6928
PD1	OBD	-25.978	-42.96	190.546	-0.4615
PD1	CBD	-24.828	-44.466	188.933	-0.678
PD1	HBD1	-25.157	-43.882	188.068	0.1994

PD1	CGD	-25.847	-45.556	189.041	0.8859
PD1	O1D	-25.66	-46.646	189.54	-0.5924
PD1	O2D	-27.021	-45.098	188.608	-0.3275
PD1	CED	-28.157	-45.94	188.828	-0.1568
PD1	HED1	-28.052	-46.471	189.773	0.1101
PD1	HED2	-28.245	-46.663	188.013	0.1199
PD1	HED3	-29.016	-45.269	188.853	0.1243
PD1	C1	-27.644	-45.876	183.518	-0.1042
PD1	H1	-27.761	-46.651	184.27	0.1233
PD1	H2	-27.942	-46.233	182.531	0.0976
PD1	H3	-28.228	-44.996	183.797	0.0923
PD2	MG	-13.531	-42.672	185.026	1.3856
PD2	CHA	-10.513	-44.016	183.829	0.0329
PD2	CHB	-15.145	-44.49	182.584	-0.5136
PD2	HHB	-15.684	-44.965	181.769	0.1628
PD2	CHC	-16.485	-42.156	186.64	-0.2011
PD2	HHC	-17.435	-41.881	187.078	0.1481
PD2	CHD	-11.836	-41.675	187.892	-0.6296
PD2	HHD	-11.296	-41.27	188.741	0.2326
PD2	NA	-12.883	-43.981	183.384	-0.3945
PD2	C1A	-11.612	-44.346	183.053	-0.0702
PD2	C2A	-11.57	-45.223	181.822	0.1459
PD2	H2A	-10.831	-44.847	181.102	-0.001
PD2	C3A	-13.006	-45.08	181.287	0.3031
PD2	H3A	-13.4	-46.061	181.022	-0.0452
PD2	C4A	-13.76	-44.492	182.476	0.2015
PD2	CMA	-13.084	-44.143	180.081	-0.4269
PD2	HMA1	-12.495	-44.524	179.239	0.0848
PD2	HMA2	-12.706	-43.151	180.353	0.0963
PD2	HMA3	-14.117	-44.033	179.757	0.125
PD2	CAA	-11.204	-46.676	182.171	0.179
PD2	HAA1	-11.948	-47.059	182.874	0.0317
PD2	HAA2	-10.241	-46.718	182.683	-0.0013
PD2	CBA	-11.14	-47.581	180.933	-0.7016
PD2	HBA1	-10.306	-47.264	180.298	0.1652

PD2	HBA2	-12.058	-47.534	180.345	0.1638
PD2	CGA	-10.948	-49.024	181.33	0.85
PD2	O1A	-11.75	-49.91	181.131	-0.5488
PD2	O2A	-9.776	-49.19	181.965	-0.3421
PD2	NB	-15.47	-43.267	184.689	-0.5602
PD2	C1B	-15.946	-43.968	183.63	0.3498
PD2	C2B	-17.404	-44.079	183.72	0.0271
PD2	C3B	-17.779	-43.402	184.858	0.0129
PD2	C4B	-16.544	-42.904	185.468	0.1226
PD2	CMB	-18.281	-44.844	182.784	-0.2921
PD2	HMB1	-17.968	-45.892	182.709	0.0738
PD2	HMB2	-18.277	-44.431	181.768	0.0916
PD2	HMB3	-19.307	-44.822	183.152	0.0874
PD2	CAB	-19.097	-43.185	185.469	-0.0687
PD2	HAB	-19.164	-43.434	186.527	0.0577
PD2	CBB	-20.17	-42.651	184.876	-0.3412
PD2	HBB1	-21.087	-42.471	185.428	0.143
PD2	HBB2	-20.156	-42.318	183.845	0.161
PD2	NC	-14.069	-42.074	186.976	-0.5634
PD2	C1C	-15.332	-41.725	187.332	0.1125
PD2	C2C	-15.31	-40.842	188.498	0.1705
PD2	C3C	-13.989	-40.685	188.84	-0.3127
PD2	C4C	-13.224	-41.486	187.886	0.5771
PD2	CMC	-16.512	-40.23	189.142	-0.377
PD2	HMC1	-17.04	-40.966	189.759	0.0902
PD2	HMC2	-17.214	-39.838	188.399	0.097
PD2	HMC3	-16.238	-39.404	189.801	0.1621
PD2	CAC	-13.422	-39.779	189.894	0.2483
PD2	HAC1	-12.967	-40.36	190.705	0.016
PD2	HAC2	-14.244	-39.227	190.357	0.0216
PD2	CBC	-12.39	-38.778	189.335	-0.3897
PD2	HBC1	-11.372	-39.166	189.425	0.0862
PD2	HBC2	-12.429	-37.834	189.879	0.135
PD2	HBC3	-12.591	-38.554	188.282	0.0863
PD2	ND	-11.634	-42.843	185.758	-0.8406
PD2	C1D	-11.08	-42.358	186.926	0.5526

PD2	C2D	-9.632	-42.61	186.938	0.0542
PD2	C3D	-9.369	-43.203	185.724	-0.3209
PD2	C4D	-10.615	-43.346	185.051	0.352
PD2	CMD	-8.679	-42.299	188.026	-0.3622
PD2	HMD1	-8.639	-43.091	188.78	0.1452
PD2	HMD2	-9.004	-41.397	188.529	0.1098
PD2	HMD3	-7.668	-42.16	187.642	0.1581
PD2	CAD	-8.31	-43.769	184.899	0.7499
PD2	OBD	-7.117	-43.839	185.103	-0.4763
PD2	CBD	-9.036	-44.334	183.601	-0.74
PD2	HBD1	-8.809	-45.399	183.51	0.2184
PD2	CGD	-8.453	-43.608	182.414	0.8305
PD2	O1D	-8.619	-42.422	182.237	-0.5531
PD2	O2D	-7.712	-44.393	181.632	-0.3576
PD2	CED	-6.932	-43.723	180.615	-0.1013
PD2	HED1	-6.68	-42.716	180.935	0.1232
PD2	HED2	-7.494	-43.672	179.687	0.1061
PD2	HED3	-6.037	-44.319	180.474	0.1172
PD2	C1	-9.498	-50.523	182.417	-0.1071
PD2	H1	-9.685	-51.247	181.623	0.084
PD2	H2	-10.114	-50.756	183.286	0.1194
PD2	H3	-8.446	-50.527	182.699	0.1146

total (PD1)	0.5668
total (PD2)	0.4332

```
elongatus_D1     MTTTLQRRESANLWERFCNWVTSTDNRLYVGWFGVIMIPTLLAATICFVIAFIAAPPVDI 60
marina_D1        MTTVLQRRESASAWERFCSFITSTNNRLYIGWFGVLMIPTLLTAVTCFVIAFIGAPPVDI 60
elongatus_D2     MTIAIGRAPAERGWFDILDDWLKRDRFVFVGWSGILLFPCAYLALGGWLTGTTFVTSWYT 60
marina_D2        MTVALGRVQ-ERGWFDVLDDWLKRDRFVFIGWSGLLLFPCAFLSIGGWFTGTTFVTSWYT 59

elongatus_D1     DGIREPVSGSLLYGNNIITGAVVPSSNAIGLHFYPIWEAAS---LDEWLYNGGPYQLIIF 117
marina_D1        DGIREPVAGSLLYGNNIITGAVVPSSNAIGLHLYPIWEAAS---LDEWLYNGGPYQLIIF 117
elongatus_D2     HGLAS----SYLEGCNFLTVAVSTPANSMGHSLLLLWGPEAQGDFTRWCQLGGLWTFIAL 116
marina_D2        HGLAS----SYLEGCNFLTAAVSTPADSMGHSLLLLWGPEARGDFTRWCQLGGMWNFVTL 115

elongatus_D1     HFLLGASCYMGRQWELSYRLGMRPWICVAYSAPLASAFAVFLIYPIGQGSFSDGMPLGIS 177
marina_D1        HYMIGCICYLGRQWEYSYRLGMRPWICVAYSAPLAATYSVFLIYPLGQGSFSDGMPLGIS 177
elongatus_D2     HGAFGLIGFMLRQFEIARLVGVRPYNAIAFSAPIAVFVSVFLIYPLGQSSWFFAPSFGVA 176
marina_D2        HGAFGLIGFMLRQFEIARLVNVRPYNAVAFSGPIAVFVSVFLMYPLGQSSWFFAPSWGVA 175

elongatus_D1     GTFNFMIVFQAEHNILMHPFHQLGVAGVFGGALFCAMHGSLVTSSLIRETTETESANYGY 237
marina_D1        GTFNFMFVFQAEHNILMHPFHMFGVAGVLGGSLFAAMHGSLVSSTLVRETTEGESANYGY 237
elongatus_D2     AIFRFLLFFQGFHNWTLNPFHMMGVAGVLGGALLCAIHGATVENTLFQDG-EGASTFRAF 235
marina_D2        SIFRFLLFVQGFHNLTLNPFHMMGVAGILGGALLCAIHGATVENTLFEDT-KDANTFSGF 234

elongatus_D1     KFGQEEETYNIVAAHGYFGRLIFQYASFNNSRSLHFFLAAWPVVGVWFTALGISTMAFNL 297
marina_D1        KFGQEEETYNIVAAHGYFGRLIFQYASFSNSRSLHFFLGAWPVVCIWLTAMGISTMAFNL 297
elongatus_D2     NPTQAEETYSMVTANRFWSQIFG--IAFSNKRWLHFFMLFVPVTGLWMSAIGVVGLALNL 293
marina_D2        SPTQSEETYSMVTANRFWSQIFG--IAFSNKRWLHFFMLFVPVTGLWASAIGLVGIALNM 292

elongatus_D1     NGFNFNHSVIDAKGN----VINTWADIINRANLGMEVMHERNAHNFPLDLA--------- 344
marina_D1        NGFNFNHSIVDSQGN----VVNTWADVLNRANLGFEVMHERNAHNFPLDLAAGESAPVAL 353
elongatus_D2     RSYDFISQEIRAAEDPEFETFYTKNLLLNEGIRAWMAPQDQPHENFVFPEEVLPRGNAL- 352
marina_D2        RAYDFVSQEIRAAEDPEFETFYTKNILLNEGLRAWMAPQDQIHENFVFPEEVLPRGNAL- 351
```

Figure S1. The amino acid sequence of the D1 and D2 subunits from *T. elongatus* and *A. marina*. Note that *T. vulcanus* PSII poessesses essentially the same amino acid sequence as *T. elongatus* PSII. D1/D2 residue pairs in each line were generated from the protein sequence alignment performed with the CLUSTAL program [1].

[1] D.G. Higgins, J.D. Thompson and T.J. Gibson, Using CLUSTAL for multiple sequence alignments, Methods Enzymol. 266 (1996) 383-402.